

Redox-Induced Solid-Solid Phase Transformation of TCNQ Microcrystals into Semiconducting Ba[TCNQ]₂ Microstructures.

S. I. Al-Saeedi¹, K. A. Al-Farhan² and A. Nafady^{2,3,*}.

¹Department of Chemistry, College of Science, Princess Nora bint Abdulrahman University, Riyadh, Saudi Arabia.

²Department of Chemistry, College of Science, King Saud University, PO Box: 2455, Riyadh – 11451, Saudi Arabia.

³Chemistry Department, Faculty of Science, Sohag University, Sohag-82524, Egypt.

Received: 19 Aug. 2014, Revised: 15 Nov. 2014, Accepted: 12 Dec. 2014.

Published online: 1 Jan. 2015.

Abstract: Microstructures of semiconducting Ba[TCNQ]₂ have been synthesized via redox-based TCNQ/Ba[TCNQ]₂ solid-solid phase transformation that takes place via one-electron reduction of solid TCNQ microcrystals, attached to an electrode surface, in the presence of an aqueous Ba²⁺_(aq) electrolyte solution. Voltammetric monitoring of the transformation process revealed that it is highly dependent on scan rate and Ba²⁺_(aq) electrolyte concentration and occurs via a rate-determining nucleation/growth process. This process involves ingress of Ba²⁺_(aq) cations into TCNQ⁻ crystal lattice at the triple phase TCNQ/TCNQ⁻_(s) | GC_(s) | Ba²⁺_(aq) electrolyte junction. SEM characterization of the morphology of the generated Ba[TCNQ]₂ material showed the formation of microstructural sheets.

Keywords: TCNQ, Redox-based, Solid-solid transformation, Nucleation-Growth, Microstructural sheets, binary Ba[TCNQ]₂.

1. Introduction

Metal-TCNQ based materials have received considerable interest over the past four decades, because of their unusual structural, optical, and conducting properties [1-7]. Potential employment of these materials in industrial and technological applications such as energy and data storage, optical and electrical media recording, sensors and catalysis, transistors and magnetic devices has fuelled many of the research activities in this area [8-19]. In recent years, a lot of efforts have been directed towards developing various synthetic routes to control the growth of these M-TCNQ micro/nano-structures, thereby tuning their inherent chemical and physical properties [20-29].

Of particular relevance to the present study is the generic electrochemical approach introduced by Bond *et al.* to induce transformations of solid TCNQ microcrystals into the corresponding 1:1 M-TCNQ systems of Group I cations (M⁺ = Na⁺, K⁺, Rb⁺, Cs⁺ as well as Cu²⁺ and Ag⁺) [30-32]

and to probe the mechanistic aspects associated with these redox-based processes. Recently Nafady *et al.* have implemented similar approaches for controlling the synthesis and fabrication of semiconducting/magnetic binary M[TCNQ]₂-based materials (M = first-row transition metal) via redox-based solid-solid phase interconversion of TCNQ-modified electrodes immersed in aqueous solution of M²⁺_(aq) electrolytes [33-38].

In contrast to the above studies, very little attention has been paid concerning binary M[TCNQ]₂(s) systems of the alkaline earth metals (Group II cations), (M²⁺ = Be²⁺, Mg²⁺, Ca²⁺, Sr²⁺, and Ba²⁺). However, in 2014 Nafady *et al.* have published the first report on electrochemical synthesis and characterization of Ca[TCNQ]₂ microstructural sheets.

As for the congener Ba[TCNQ]₂, it was chemically synthesized by Melby and co-workers via mixing excess BaI₂ in boiling methanol with hot solution of TCNQ in acetonitrile. The formed purple crystals of Ba[TCNQ]₂

*Corresponding author e-mail: anafady@ksu.edu.sa

exhibited resistivity (8×10^5 Ohm cm) in the range of semiconductors [39]. After that only sporadic interest was shown in form of measuring the solid-state reflection spectra of $\text{Ba}[\text{TCNQ}]_2$ by Oohashi and Sakata [40] or the electronic absorption spectra (UV/Vis) of both $\text{Ba}[\text{TCNQ}]_2$ and $\text{Ca}[\text{TCNQ}]_2$ at low temperatures [41]. Importantly, data obtained from these measurements were identical to those obtained for KTCNQ, thereby confirming the presence of TCNQ^- in these materials [42-46].

In the present contribution, we describe detailed electrochemical, spectroscopic (IR and Raman) and microscopic (SEM and EDX) characterization of the solid-solid phase transformation of TCNQ-modified electrodes into the corresponding semiconducting $\text{Ba}[\text{TCNQ}]_2$ microstructures when immersed in aqueous $\text{Ba}^{2+}_{(\text{aq})}$ electrolytes.

2. Experimental Section

2.1 Materials and Electrochemical Synthesis of $\text{Ba}[\text{TCNQ}]_2$

Analytical grade hydrated $\text{Ba}(\text{NO}_3)_2 \cdot x\text{H}_2\text{O}$, TCNQ (98%) (Aldrich) and acetonitrile (HPLC grade, Omnisolv) were used as received from the suppliers. Electrochemical synthesis of $\text{Ba}[\text{TCNQ}]_2$ is performed via reductive electrolysis (10-15 min) of a TCNQ-modified ITO electrode, immersed in an aqueous $\text{Ca}(\text{NO}_3)_2$ solution (0.10 M, pH = 6.8) at constant applied potential ($E_{\text{appl}} = -0.15$ V) versus Ag/AgCl. Having neutral electrolyte solution is essential to avoid interference by proton (H^+) intercalation that could happen if the solution is highly acidic. The dark blue solid, formed on the surface of the ITO electrode, was gently rinsed with deionized water, and then dried initially under a stream of nitrogen gas for 10 min, followed by vacuum drying overnight. The solid was characterized by FTIR, Raman spectroscopy, and scanning electron microscopy (SEM). Both chemically and electrochemically prepared solids have identical spectroscopic characterization, confirming the presence of TCNQ^- in the solids.

2.2 Electrochemistry

Aqueous solutions of $\text{Ba}(\text{NO}_3)_2$ used for electrochemical measurements were prepared using water purified in a Millipore System (resistivity $18.2 \text{ M}\Omega \text{ cm}$). Electrochemical studies were performed with an Autolab PGSTAT100 (ECO-Chemie) workstation and a standard three-electrode cell configuration. For voltammetric and potential-step experiments, glassy carbon (GC) disk (3 mm diameter, Bionalytical Systems) and indium tin oxide (ITO)-coated glass ($0.06\text{-}0.1 \text{ cm}^2$ area) having a $10 \text{ }\Omega/\text{sq}$ sheet resistance (as quoted by the manufacturer Prazisions Glas and Optik GmbH) were used as the working electrodes. The procedures employed for polishing these electrodes are described elsewhere [33]. The reference

electrode was an aqueous Ag/AgCl (3 M KCl, Bioanalytical Systems) and the counter electrode was made from platinum mesh. A stream of N_2 gas was used to sparge the aqueous solutions in which chemically modified TCNQ electrodes were placed, and a flow of this gas was maintained above the solution during the course of electrochemical experiments.

2.3 Physical Measurements

Infrared (IR) and Raman spectroscopy, scanning electron microscopy (SEM), and energy-dispersive X-ray (EDAX) measurements were carried out as previously reported [33].

3. Result and discussion

3.1 Voltammetric Monitoring of $\text{TCNQ}/\text{Ca}[\text{TCNQ}]_2$ Solid-Solid phase Transformation

3.1.1. Reduction of Solid TCNQ in the Presence of $\text{Ba}^{2+}_{(\text{aq})}$ Electrolyte

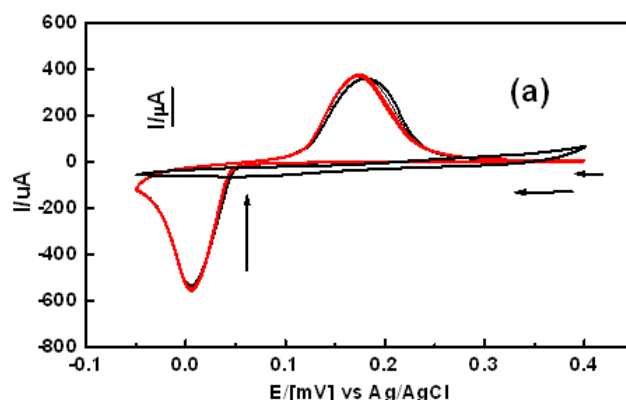


Figure 1: Cyclic voltammograms obtained with a scan rate of 20 mV s^{-1} for the fifth cycle of the potential over the range of 0.45 to -0.1 V at (a) bare GC surface and (b) TCNQ-modified GC disk electrode (mechanical attachment) in contact with $0.1 \text{ M Ba}(\text{NO}_3)_{2(\text{aq})}$ electrolyte.

Figure 1 shows the cyclic voltammograms obtained at a scan rate of 20 mV s^{-1} over the potential range of 0.45 to -0.10 V vs. Ag/AgCl with bare and TCNQ-modified GC electrodes (via mechanical attachment method) when placed in contact with $0.10 \text{ M Ba}(\text{NO}_3)_{2(\text{aq})}$ electrolyte. As expected, $\text{Ba}^{2+}_{(\text{aq})}$ cations are very stable and do not undergo any redox processes over the designated potential range when a bare GC electrode is used (Fig. 1). Therefore, the observed electrochemical activity with TCNQ-modified GC electrode (Fig. 1) is attributed to the one-electron reduction of TCNQ into TCNQ^- and its immediate transformation into the corresponding Ba-TCNQ based material via intercalation of $\text{Ba}^{2+}_{(\text{aq})}$ ions into the crystal lattice of TCNQ^- .

As noted with the structurally and conceptually related $\text{TCNQ}/\text{Ca}[\text{TCNQ}]_2$ conversion processes [33-36], the voltammogram comprises well-defined and markedly

separated reduction and oxidation components, having peak potentials E_p^{red} and E_p^{ox} at 0.005 and 0.175 V respectively. A large peak- to-peak separation ($\Delta E_p = E_p^{\text{ox}} - E_p^{\text{red}} = 170$ mV) is consistent with expectation for an electrochemically-irreversible TCNQ/Ba[TCNQ]₂ solid-solid phase conversion governed by nucleation-growth kinetics [47-50]. The fact that ΔE_p of the Ba-TCNQ system is very close to that reported for the congener Ca[TCNQ]₂ ($\Delta E_p = 180$ mV) [30], it implies that the two systems are kinetically similar. This is virtually acceptable since both Ba²⁺ and Ca²⁺ cations do not form charge-transfer complexes with TCNQ as noted for CuTCNQ [31] and other divalent transition metal cations M[TCNQ]₂ systems ($M^{2+} = \text{Mn, Fe, Co and Ni}$) [33-36].

Although ΔE_p is generally considered as a kinetic parameter related to nucleation overpotential, it has been proven to have a thermodynamic origin, arising from a “miscibility gap” between the two (parent/product) phases as pointed out by Scholz *et al.* in their solid state work at the “triple phase junction” [51-53]. Thus, on the basis the conceptual similarity between Ba-TCNQ, Ca-TCNQ, and other M-TCNQ systems (M = Group I cations or first row transition metals) it can be concluded that both nucleation-growth and miscibility gap theories are applicable and can be used to interpret the observation of large ΔE_p for the TCNQ/Ba-TCNQ interconversion. Thus, the implication of the large ΔE_p in the Ba-TCNQ system indicate a significant difference in the crystal structure of the parent TCNQ and the electrochemically generated Ba-TCNQ as seen for Cs-TCNQ system which showed the biggest ΔE_p value of 250 mV among Group I cations [37].

Unlike Ca[TCNQ]₂ congener, which showed dramatic attenuation in the peak current heights upon progressive cycling of potential (max 10 cycles), the TCNQ/Ba[TCNQ]₂ transformation is persistent with very minimal decrease in peak current heights during the course of cycling the potential. As illustrated in Fig. 2, even upon reaching 50 redox cycles, the current heights and therefore the charges (Q_{red} and Q_{ox}) are slightly decreased to almost 5~10 % of their initial values. This behavior implies that the electrochemically generated Ba-TCNQ is less soluble in aqueous media than the congener Ca[TCNQ]₂ material under redox cycling conditions. Significantly, the detection of only one oxidation process, even after 50 redox cycles attests that only one phase of Ba[TCNQ]₂-based material is formed.

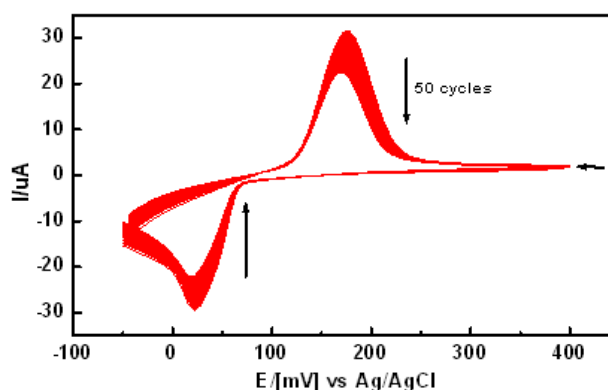
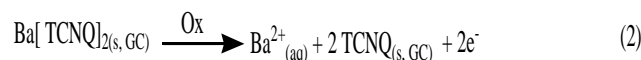


Figure 2: Cyclic voltammograms (first 50 cycles of potential) obtained at a scan rate of 50 mV s⁻¹ when a TCNQ-modified GC electrode prepared via the mechanical attachment method is placed in contact with 0.10 M Ba(NO₃)_{2(aq)} electrolyte and scanned over the potential range of 0.45 to -0.050 V.

In view of these voltammetric results, the reactions associated with this redox-based, chemically reversible, TCNQ/Ba[TCNQ]₂ transformation process can be described by eqs. 1 and 2 as follow:



As seen in the Ca-TCNQ case and related TCNQ/M[TCNQ]₂(H₂O)₂ (M = Mn²⁺, Fe²⁺, Co²⁺, Ni²⁺) [33-36], the ingress of Ba²⁺_(aq) cations into the TCNQ/TCNQ⁻ crystal lattice (eq1) and its egress upon oxidation (eq 2) is expected to take place more facile in the smaller-sized mechanically attached microparticles of TCNQ than in the case when using the considerably larger crystals produced by the drop casting method.

3.2. Evidence for Nucleation/Growth Kinetics in TCNQ/Ba[TCNQ]₂ Interconversion.

3.2.1. Scan rate and switching potential effects.

Figure 3 shows cyclic voltammograms obtained at designated scan rates ($v = 5 - 40$ mV) for the TCNQ/Ba[TCNQ]₂ solid-solid phase transformation process when the TCNQ-modified GC electrode (mechanical attachment) is placed in contact with 0.1 M Ba²⁺_(aq) ions. Analysis of the extracted voltammetric data (Table 1) demonstrates that both E_p^{red} and E_p^{ox} are markedly influenced by increasing the scan rate from 5.0 to 40 mV s⁻¹. Thus, E_p^{red} shifts to more negative by 32 mV while E_p^{ox} becomes more positive (34 mV shift) over this scan rate range. $W_{1/2}$ and ΔE_p also are significantly increased but E_m remains almost constant, as expected for a thermodynamically significant parameter. The dependence

of the aforementioned voltammetric parameters on scan rate is indicative of nucleation/growth kinetics as reported for other M-TCNQ systems [33-36, 47-50].

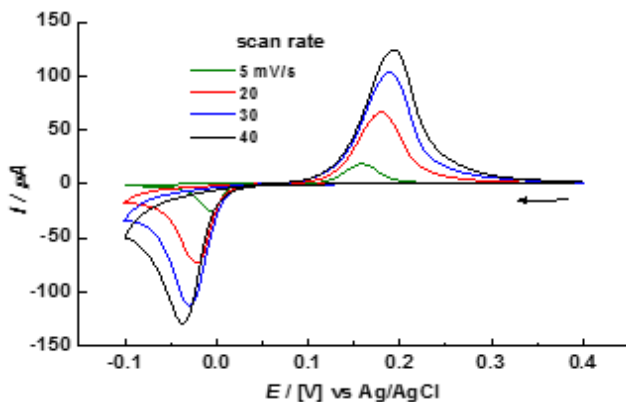


Figure 3: Cyclic Voltammograms obtained with TCNQ-modified GC electrode (mechanical attachment) in contact with 0.1 M $\text{Ba}(\text{NO}_3)_2(\text{aq})$ solution at designated scan rates.

An additional diagnostic feature for rate-determining nucleation-growth kinetics in the electrochemically induced TCNQ/M-TCNQ conversion processes is the observation of current loops in cyclic voltammograms at the onset of the reduction or oxidation components [47,49]. This is clearly evident in Figure 4, when the forward scan direction is reversed the foot of reduction process.

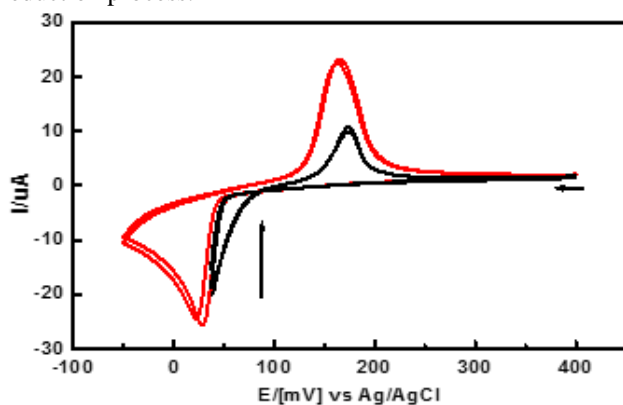


Figure 4: Cyclic Voltammograms obtained with TCNQ-modified GC electrode in contact with 0.1 M $\text{Ba}^{2+}(\text{aq})$ solution at scan rate of 0.020 V s^{-1} .

3.2.2. Chronoamperometry.

Figure 5 shows a typical current-time ($i-t$) curve obtained by double potential step chronoamperometry for a TCNQ-modified GC electrode in the presence of 0.1 M $\text{Ca}^{2+}(\text{aq})$ electrolyte over the potential range (0.45 to -0.10 V). This behavior is indicative for the presence of nucleation-growth kinetics.

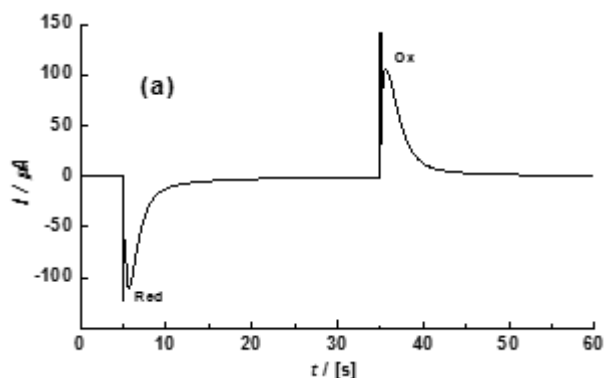


Figure 5: Double-potential step chronoamperograms obtained when a GC electrode modified with microcrystals of TCNQ (mechanical attachment) is placed in contact with 0.1 M $\text{Ca}(\text{NO}_3)_2(\text{aq})$: (a) $i-t$ transient obtained when the potential is initially stepped from $E_i = 400$ to $E_{\text{red}} = -10 \text{ mV}$ for 30 s to induce reduction and then back to $E_{\text{ox}} = 165 \text{ mV}$ to induce oxidation

Taken together, the combined voltammetric and chronoamperometric data clearly demonstrate that the redox-based TCNQ/ $\text{Ba}[\text{TCNQ}]_2$ transformation represents a chemically reversible process in which the solid-solid phase change is governed by nucleation-growth kinetics as seen with other $\text{M}^{n+}[\text{TCNQ}]_n$ systems ($\text{M} = \text{Mn}^{2+}, \text{Fe}^{2+}, \text{Co}^{2+}, \text{Ni}^{2+}, \text{Cu}^{2+}, \text{Ca}^{2+}, \text{Ag}^+, \text{Li}^+, \text{Na}^+, \text{K}^+, \text{Rb}^+$ and Cs^+ $n = 1$ or 2) [30-36, 47-50].

3.3. Characterization of the Electrochemically-Synthesized $\text{Ca}[\text{TCNQ}]_2$ Material.

3.3.1. IR spectroscopy.

Inspection of the IR spectra of the electrochemically generated Ba-TCNQ solid revealed the presence of two bands in the $\nu(\text{C}\equiv\text{N})$ region at 2205 and 2173 cm^{-1} , a single stretch for $\nu(\text{C}=\text{C})$ at 1506 cm^{-1} , and a sharp $\delta(\text{C}-\text{H})$ bending band at 819 cm^{-1} . These bands are in excellent agreement with those reported for $\text{Ca}[\text{TCNQ}]_2$, $\text{Ba}[\text{TCNQ}]$ and KTCNQ [39,43,44] and the binary $\text{M}[\text{TCNQ}]_2(\text{H}_2\text{O})_2$ family [33-36], thereby confirming the presence of $\text{TCNQ}^{\cdot-}$ anion radical in the generated material. Similar to the reported $\text{Ba}[\text{TCNQ}]_2$, the absence of the characteristic broad bands for water in the $3400\text{-}3350 \text{ cm}^{-1}$ region, attests that the electrochemically-produced material does not contain coordinated water molecules.

3.3.2. Raman Spectroscopy.

The Raman spectra of Ba-TCNQ solid shows four characteristic vibrations modes of $\text{TCNQ}^{\cdot-}$ radical anion at 1205 , 1395 , 1603 , and 2215 cm^{-1} , respectively. The red shift (57 cm^{-1}) in the 1454 cm^{-1} band, attributed to the $\text{C}=\text{C}$ ring stretching mode of TCNQ, is as found for congener Ca-TCNQ and other binary $\text{M}[\text{TCNQ}]_2$ ($\text{M}^{2+} = \text{Mn}, \text{Fe}, \text{Co}, \text{Ni}$) [33-37] materials and therefore gives full support for

the presence of TCNQ⁻ in the electrochemically synthesized Ba[TCNQ]₂ material.

3.3.3. Energy dispersive X-ray.

EDAX elemental analysis of Ba[TCNQ]₂ solid generated by reductive bulk electrolysis of TCNQ-modified ITO electrodes for 10-15 mins at applied potential (E_{app}) of -0.15 V vs Ag/AgCl (Fig. 6) revealed the presence of calcium as well as carbon and nitrogen, as expected for the formation of Ba[TCNQ]₂. In view of the combined electrochemical and spectroscopic (IR, Raman, EDX) data, it is clearly evident that electrochemical reduction of TCNQ microcrystals attached to either GC or ITO working electrode and immersed in aqueous Ca²⁺_(aq) electrolyte ions gave rise to a single phase of binary Ba[TCNQ]₂ solid.

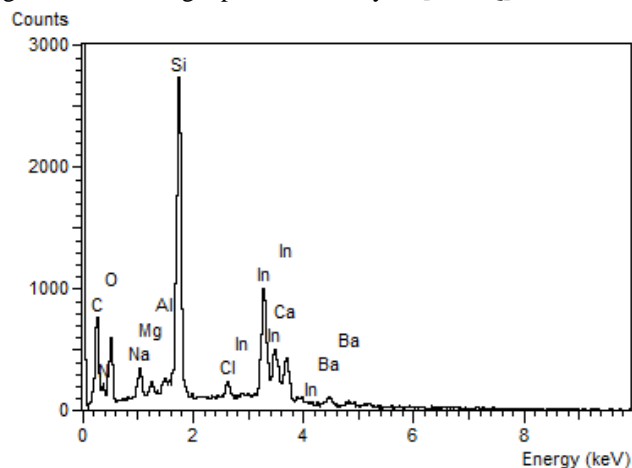


Figure 6: EDAX analysis of Ba-TCNQ sample.

3.4. SEM Probing of the TCNQ/Ba[TCNQ]₂ Transformation Process.

3.4.1. Drop casting method.

Figure 7a shows SEM image of a typical rhombus-shaped crystal of parent TCNQ immobilized on an ITO surface via the drop casting method before introducing into the electrochemical cell that contains 0.1 M Ba²⁺_(aq) electrolyte solution. SEM images of the electrochemically-synthesized Ba[TCNQ]₂ material are provided in Figures 7b-d. As found with other binary M[TCNQ]₂(H₂O)₂ (M²⁺ = Mn, Fe, Co, and Ni) [33-36], the whole faces (top, bottom and edges) of the parent TCNQ crystals are completely covered with thin rectangular sheets of Ca[TCNQ]₂ crystals as shown in the low magnification image in Fig. 7b. At higher magnification (Fig 7c and d) the SEM images clearly illustrate that these microstructured architectures are interconnected, giving rise to a network of densely packed, thin, 2-D/3-D micro-sized rectangular rods/sheets. The average size of these sheets is 0.5 to 2.0 μm in length and ~50-100 nm thickness. Although the majority of these thin sheets have random growth, some prefer to grow upwards.

Importantly, since most of the thin sheets are preferentially

derived from the growth along the surface (edges, top and presumably base) of the large TCNQ crystals rather than through the middle, the basic architecture of TCNQ crystal can remain intact. From energetic perspective, the triple phase junction, namely TCNQ/TCNQ⁻_(s) | ITO_(s) | Ca²⁺_(aq) electrolyte [47,50-53] may represent the location for initial nucleation sites, which proceeds with time then preferentially grow from the base of TCNQ crystal along the edges to reach the top the TCNQ crystal. This type of "network" nucleation-growth is probably accelerated by the semiconducting nature of the Ca[TCNQ]₂ material [39, 46].

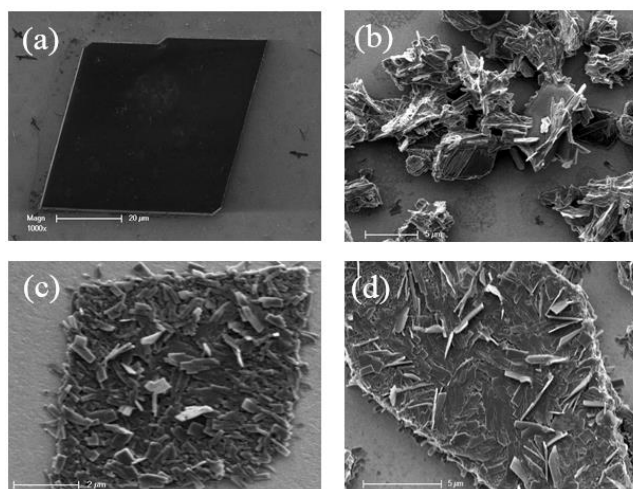


Figure 7: (a) SEM image of a single crystal of TCNQ present on a TCNQ-modified ITO electrode prepared via the drop casting method. (b) SEM image of Ba[TCNQ]₂ formed by reductive electrolysis for 10 min at -0.10 V of TCNQ-modified ITO.

electrode, immersed in 0.1 M Ba(NO₃)_{2(aq)} electrolyte. Images (c and d) show top-view of the crystals in image (b), but at higher magnifications.

3.4.2. Mechanical attachment method.

Reductive electrolysis experiments undertaken with ITO surfaces modified with solid TCNQ via the mechanical attachment method produced nearly the same morphology of Ba[TCNQ]₂ microstructures as the drop casting method, although the initial morphology of parent TCNQ crystals in both cases are dramatically different. As can be seen in Fig. 8a, the densely packed amorphous thin layer of TCNQ microparticles are converted, after 10 minutes of reductive electrolysis, into a compact layer of randomly oriented microstructural sheets (Fig. 8b) of Ba[TCNQ]₂. At higher magnification (Fig. 8c, 8d), these sheets appear as square/rectangle thin rods or plates. Although these SEM results are very similar to those obtained for the congener Ca[TCNQ]₂ materials, they are totally different in morphologies and crystals sizes than those of parent TCNQ and the conceptually related (1:1) MTCNQ (M = Li⁺, Na⁺, K⁺, Rb⁺, and Cs⁺) [30] and binary M[TCNQ]₂(H₂O)₂ (M²⁺ = Mn, Fe, Co, Ni) complexes [33-36] under similar

conditions. These marked morphology differences (microstructural rectangular/square thin sheets versus needle-shaped nanowires/rods) underscores the important role of the metal cation in controlling the kinetics of transformation as well as the extent and direction of growth in these redox-based solid-solid interconversion processes.

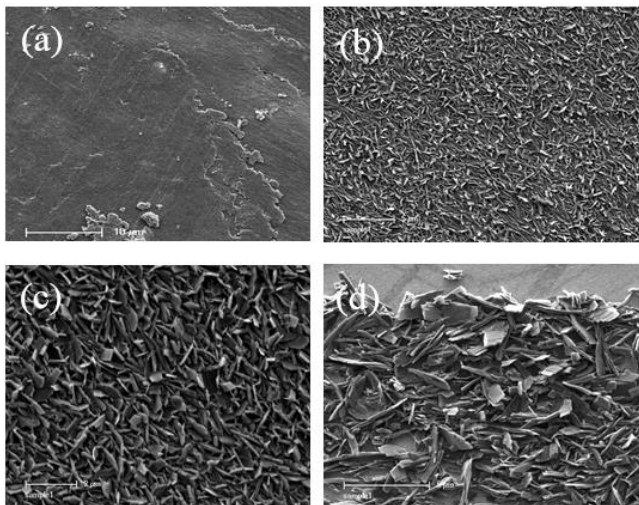


Figure 8: (a) SEM image of a TCNQ-modified ITO surface via mechanical attachment method before introduced into the electrochemical cell. (b) SEM image of Ba[TCNQ]₂ micro-sheets formed by reductive electrolysis for 10 min at -0.10 V of solid TCNQ adhered to an ITO electrode surface as image (a) when placed in contact with 0.1 M Ba(NO₃)_{2(aq)} electrolyte. Images (c and d) are as in image (b) but higher magnifications.

4. Conclusion

We have employed solid-state electrochemical approaches, developed for probing the redox-based transformation of solid TCNQ into the conceptually related M-TCNQ systems ($M^+ = \text{Li}^+, \text{Na}^+, \text{K}^+, \text{Rb}^+$ and Cs^+) and binary $M[\text{TCNQ}]_2(\text{H}_2\text{O})_2$ ($M^{2+} = \text{Mn}^{2+}, \text{Fe}^{2+}, \text{Co}^{2+}$, and Ni^{2+}) to synthesize microstructural square/rectangular sheets of semiconducting Ba[TCNQ]₂ material. This is achieved by one-electron reduction of TCNQ-modified electrodes into the corresponding TCNQ⁻ radical anion coupled with ingress of Ba²⁺_(aq) ions, from the bulk solution, into the crystal lattice. The underlying TCNQ/Ba[TCNQ]₂ solid-solid transformation is controlled by initial nucleation at the triple phase: GC or ITO_(s) | (TCNQ_(s)/TCNQ⁻) | Ba²⁺_(aq) junction followed by fast growth kinetics.

Consistent with congener Ca[TCNQ]₂ and other M-TCNQ systems of Group I and divalent transition metal cations, the TCNQ/Ba[TCNQ]₂ voltammetric behavior is highly dependent on scan rate, Ba²⁺_(aq) electrolyte concentration, and the method of electrode modification. A significant outcome of the present study is the provision of facile procedures and easy access to superior electrochemical routes that allow not only controllable

synthesis, characterization, and fabrication of binary M-TCNQ systems of alkaline earth metals (e.g., Be²⁺, Mg²⁺, Sr²⁺ and Ba²⁺) but also understanding of the mechanistic aspects associated with their formation.

Acknowledgements

The authors would like to extend their sincere appreciation to Scientific Research at King Saud University for funding through the Research Group Project no RGP-VPP-236.

References

- [1] O. H. LeBlanc, *J Chem Phys* **42**, 4307-4308, (1965).
- [2] L. Ballester, A. Gutierrez, M. F. Perpina, M. T. Azcondo, *Coord Chem, Rev* **190-192**, 447-470, (1999).
- [3] H. Miyasaka, C. S. Campos-Fernandez, R. Clerac, K. R. Dunbar, *Angew. Chem. Int. Ed* **39**, 3831-3835, (2000).
- [4] K. I. Pokhodnya, N. Petersen, J. S. Miller, *Inorg Chem* **41**, 1996-1997, (2000).
- [5] N. Kuroda, T. Sugimoto, M. Hagiwara, Hasanudin, K. Ueda, T. Tada, H. Uozaki, N. Toyota, I. Mogi, K. Watanabe, M. Motokawa, *Synth. Met.* **133-134**, 535-537, (2003).
- [6] K. Ueda, M. Takahashi, H. Tomizawa, E. Miki, C. Faulmann, *J. Mol. Struct.* **751**: 12-16, (2005).
- [7] R. Jain, K. Kabir, J. B. Gilroy, K. A. R Mitchell, K. C. Wong, R. G. Hicks, *Nature* **445**, 291-294, (2007).
- [8] X. L. Mo, G. R. Chen, Q. J. Cai, Z. Y. Fan, H. H. Xu, Y. Yao, J. Yang, H. H. Gu, Z. Y. Hua, *Thin Solid Films* **436**, 259-263, (2003).
- [9] J. S. Kim, O. K. Cho, K. S. Min, K.Y. Park, *Synth. Met.* **71**, 2215-2216, (1995).
- [10] J. S. Kim, O. K. Cho, K. S. Min, K. Y. Park, *Mol. Cryst. Liq. Cryst.* **267**, 375-380, (1995).
- [11] S. Yamaguchi, R. S. Potember, *Synth. Met.* **78**, 117-126, (1996).
- [12] C. B. Ran, H. L. Peng, W. Zhou, X. C. Yu, Z. F. Liu, *J. Phys. Chem. B* **109**, 22486-22490, (2005).
- [13] H. L. Peng, C. B. Ran, X. C. Yu, R. Zhang, Z. F. Liu, *Adv. Mater.* **17**, 459-464, (2005).
- [14] A. R. Brown, D. M. Deleeuw, E. J. Lous, E. E. Havinga, *Synth. Met.* **66**, 257-261, (1994).
- [15] E. Menard, V. Podzorov, S. H. Hur, A. Gaur, M. E. Gershenson, J. A. Rogers, *Adv. Mater.* **16**, 2097-2101, (2004).
- [16] M. Cano, B. Palenzuela, R. Rodriguez-Amaro, *Electroanalysis* **18**, 1068-1074, (2006).

- [17] X. Llopis, A. Merkoci, M. d'Valle, S. Alegret, *Sens Actuators B* **107**, 742-748, (2005).
- [18] P. C. Pandey, S. Upadhyay, S. Sharma, *Electroanalysis* **15**, 1115-1119, (2003).
- [19] A. Yasuda, J. Seto, *J. Electroanal. Chem.* **247**, 193-202, (1988).
- [20] R. Muller, S. De Jonge, K. Myny, D. J. Wouters, J. Genoe, P. Heremans, *Solid-State Electronics* **50**, 601-605, (2006).
- [21] T. Shang, F. Yang, W. Zheng, C. Wang, *Small* **2**, 1007-1009, (2006).
- [22] A. P. O'Mullane, N. Fay, A. Nafady, A. M. Bond, *J. Am. Chem. Soc.* **129**, 2066-2073, (2007).
- [23] A. P. Alivisatos, *Science* **271**, 933-937, (1996).
- [24] C. Burda, X. Chen, R. Narayanan, M. A. El-Sayed, *Chem. Rev.* **105**, 1025-1102, (2005).
- [25] A. K. Neufeld, A. P. O'Mullane, A. M. Bond, *J. Am. Chem. Soc.* **127**, 13846-13853, (2005).
- [26] A. Nafady, A. M. Bond, A. Bilyk, A. R. Harris, A. I. Bhatt, A. P. O'Mullane, R. De Marco, *J. Am. Chem. Soc.* **129**, 2369-2382, (2007).
- [27] R. A. Heintz, H. Zhao, X. Ouyang, G. Grandinetti, J. Cowen, K. R. Dunbar, *Inorg. Chem.* **38**, 144-156, (1999).
- [28] C. Avendano, Z. Zhang, A. Ota, H. Zhao, K. R. Dunbar, *Angew. Chem.* **50**, 6543-6547, (2011).
- [29] Z. Zhang, H. Zhao, H. Kojima, T. Mori, K. R. Dunbar, *Chem. Eur. J.* **19**, 3348-3357, (2013).
- [30] A. M. Bond, S. Fletcher, P. G. Symons, *Analyst* **123**, 1891-1904, (1998).
- [31] A. K. Neufeld, I. Madsen, A. M. Bond, C. F. Hogan, *Chem. Mater.* **15**, 3573-3585, (2003).
- [32] A. R. Harris, A. Nafady, A. P. O'Mullane, A. M. Bond, *Chem. Mater.* **19**, 5499-5509, (2007).
- [33] A. Nafady, A. P. O'Mullane, A. M. Bond, A. K. Neufeld, *Chem. Mater.* **18**, 4375-4384, (2006).
- [34] A. Nafady, A. M. Bond, *Inorg. Chem.* **46**, 4128-4137, (2007).
- [35] A. Nafady, A. M. Bond, A. Bilyk, *J. Phys. Chem. C.* **112**, 6700-6709, (2008).
- [36] A. Nafady, A. M. Bond, A. P. O'Mullane, *Inorg. Chem.* **48**, 9258-2970, (2009).
- [37] A. Nafady, A. M. Bond, V. Qu, L. L. Martin, *J. Solid State Electrochem.* **17**, 1609-1620, (2013).
- [38] X. Qu, A. Nafady, A. Mechler, J. Zhang, A. R. Harris, A. P. O'Mullane, L. L. Martin, A. M. Bond, *J. Solid State Electrochem.* **12**, 739-746, (2008).
- [39] L. R. Melby, R. J. Harder, W. R. Hertler, W. Mahler, R. E. Benson, W. E. Mochel, *J. Am. Chem. Soc.* **84**, 3374-3387, (1962).
- [40] Y. Oohashi, T. Sakata, *Bull. Chem. Soc. Jpn.* **46**, 3330-3335, (1973).
- [41] M. Michaud, C. Carlone, N. K. Hota, J. Zauhar, *Chem. Phys.* **36**, 79-84, (1979).
- [42] N. Sakai, I. Shirovani, S. Minomura, *Bull. Chem. Soc. Jpn.* **45**, 3314-3328, (1972).
- [43] M. S. Khatkale, J. P. Devlin, *J. Phys. Chem.* **83**, 1636-1640, (1979).
- [44] H. Zhao, R. A. Heintz, X. Ouyang, K. R. Dunbar, C. F. Campana, R. D. Rogers, *Chem. Mater.* **11**, 736-746, (1999).
- [45] E. B. Vickers, T. D. Selby, M. S. Thorum, M. L. Taliaferro, J. S. Miller, *Inorg. Chem.* **43**, 6414-6420, (2004).
- [46] M. Oyama, R. D. Webster, M. Suarez, F. Marken, R. G. Compton, *J. Phys. Chem. B* **102**, 6588-6595, (1998).
- [47] A. M. Bond, S. Fletcher, F. Marken, S. J. Shaw, P. G. Symons, *J. Chem. Soc. Faraday. Trans.* **92**, 3925-3933, (1996).
- [48] M. F. Suarez, A. M. Bond, R. G. Compton, *J. Solid State Electrochem* **4**, 24-33, (1999).
- [49] S. Fletcher, C. S. Halliday, D. Gates, M. Westcott, T. Lwin, G. Nelson, *J. Electroanal. Chem.* **159**, 267-285, (1983).
- [50] M. F. Suarez, F. Marken, R. G. Compton, A. M. Bond, W. Miao, C. L. Raston, *J. Phys. Chem. B* **103**, 5637, (1999).
- [51] F. Scholz, M. Lovric, Z. Stojek, *J. Solid State Electrochem.* **1**, 134-142, (1997).
- [52] T. Grygar, F. Marken, U. Schröder, F. Scholz, *Collect Czech Chem. Commun.* **67**, 163-208, (2002).
- [53] E. Bak, M. Donten, Z. Stojek, F. Scholz, *Electrochem. Comm.* **9**, 386-392, (2007).